



# Numerical and experimental study of mixed flow pump as turbine for remote rural micro hydro power plant application

Sarid Mejiartono <sup>a, \*</sup>, Muhammad Fathul Hikmawan <sup>b</sup>, Aditya Sukma Nugraha <sup>b, c</sup>

<sup>a</sup> Faculty of Mechanical and Aerospace Engineering, Bandung Institute of Technology  
Jl. Ganesa No.10, Lb. Siliwangi, Bandung, 40132, Indonesia

<sup>b</sup> Research Center for Smart Mechatronics, National Research and Innovation Agency (BRIN)  
Kawasan Bandung Cisit, Jl. Sangkuriang, Dago, Coblong, Bandung, 40135, Indonesia

<sup>c</sup> Department of Mechanical Engineering, National Taiwan University of Science and Technology  
Taipei, 10672, Taiwan

Received 18 July 2022; 1<sup>st</sup> revision 11 October 2022; 2<sup>nd</sup> revision 29 October 2022; 3<sup>rd</sup> revision 12 November 2022;  
4<sup>th</sup> revision 18 November 2022; Accepted 21 November 2022; Published online 29 December 2022

## Abstract

The use of a pump as opposed to a turbine/pump as turbine (PAT) for off-grid electrification applications is one of the important ways to be considered in efforts to equalize electrical energy in Indonesia. The main problem in PAT applications is how to predict pump performance if applied as a turbine to find out its best characteristics and efficiency points. This study discusses a method to find pump performance specifications when using a pump with a mixed flow type as a turbine for micro hydro power plants. The numerical method by utilizing computational fluid dynamics (CFD) based software simulations that have been proven to be accurate according to previous studies was selected for use in obtaining predictions of the pump characteristics as turbines. Then the PAT characteristics of the CFD simulation results are validated by conducting direct testing. The results of the CFD numerical simulation using ANSYS Fluent software show the performance curve of a mixed flow pump operated as a turbine at various rotating speeds. The highest efficiency for each rotating speed ranges from 35-40 %. The test results directly show the PAT characteristics, that the performance range is close to the numerical simulation results with a difference of 10 %.

Copyright ©2022 National Research and Innovation Agency. This is an open access article under the CC BY-NC-SA license (<https://creativecommons.org/licenses/by-nc-sa/4.0/>).

Keywords: pump as turbine (PAT); micro hydro power plant; computational fluid dynamics (CFD).

## 1. Introduction

The improvement and equitable distribution of the economic development of each country will not be able to be realized without building its energy availability. Electrical energy is one of the most vital and necessary forms of energy in society today. The need for electrical energy in each region will inevitably continue to be needed along with the growth of the needs of its population. Study [1] stated that Indonesia's energy needs in 2025 are 170.8, 154.7, and 150.1 MTOE, respectively, based on energy mix (EM), sustainable development (SD), and low carbon (LC) scenarios. Many studies are also carried out to predict the addition of energy needs in every region. In [2] has conducted research on the

prediction of electricity demand by utilizing artificial neural networks (ANN). In Indonesia, research on predicting energy consumption has been conducted by [3][4] recently. On the other hand, the problem of the availability of fossil energy continues to decrease and certainly cannot be renewed anymore. One of the keys to answering all these problems is renewable energy. Various studies continue to be carried out in developing technology to be able to absorb and utilize renewable energy as much as possible. The renewable energy potentials owned by each region continue to be sought and studied to be utilized as well as possible. Indonesia, with its location and geographical conditions, has the potential for very abundant renewable energy resources, one of which is water resources. With its heavy rainfall and topographical conditions, Indonesia was awarded more than 5,000 Watersheds. The utilization of these water resources can be done

\* Corresponding Author. Tel: +62-81275730779, +62-85643591995  
E-mail: sarid.mejiartono@gmail.com

by building hydroelectric power plants and micro hydro power plants to take advantage of small potentials in remote areas. Various studies on potentials in watersheds in Indonesia have been carried out, some of which have been carried out by [5][6][7].

The area, location, and geographical conditions of Indonesia, on the other hand, are one of the factors inhibiting the equitable fulfillment of electrical energy throughout its territory, apart from the factor of the amount of energy that can be produced by electricity companies. The micro-hydroelectric power plant scheme by utilizing pumps as turbines (PAT) for remote off-grid electrification can be used as a way to equalize electrical energy in Indonesia. The PAT system for micro hydro power plants in remote areas is very promising, especially because it is very economical. Several studies on the techno-economical, costs, and advantages of PAT applications for micro hydro power plants have been carried out, among others by [8][9]. In addition, PAT has various other advantages, including the ease of availability, availability for various heads and flows, simple construction, and it also allows one to significantly reduce design and maintenance costs compared to traditional turbine applications.

In general, PAT has a lower efficiency when compared to conventional water turbines. However, in the application of PAT for micro hydro power plants in remote areas, efficiency is not the main criterion in its selection. The efficiency problem, in this case, can be solved slightly by means of operating the PAT around its maximum efficiency point. However, the main and most challenging problem in PAT applications is how to predict performance at its best efficiency point. Several studies have been conducted related to efforts to obtain predictions of pump performance when used as a turbine. Research conducted by [10] pays attention to the benefits of computational fluid dynamics (CFD) for studying PAT. [11] presents a detailed analysis of three-dimensional flow and predicts pump as turbine (PAT) performance. The speed triangle in turbine mode is calculated analytically and evaluated numerically by CFD. The rate characteristics of the internal flow have also been investigated by [12] performed on conventional centrifugal pumps using CFD software. In his research, the SST  $k-\omega$  turbulence model was used. That is a combination of the standard  $k-\varepsilon$  model and the standard  $k-\omega$  model. The advantage of using this combined model is that it can capture small flows in viscous layers with the advantages of the standard  $k-\varepsilon$  model in the region of the persistent turbulent core [13] has conducted an experimental study to determine the effect of viscosity on the performance of the PAT system. Prediction of PAT performance when working at different rotational speeds is carried out by [14]. Research studying irreversible energy losses in PAT was introduced by [15] based on the point of view of the second law of thermodynamics as well as the theory of entropy generation [16]. It has also introduced a method for predicting PAT performance based on theory and numerically in a *single stage*

centrifugal pump operated as a turbine. The surface roughness effect of the impeller/pump blade used as a turbine has been studied by [17]. Another study introducing a new theoretical method for predicting the best efficiency points of PAT has been worked out by [18], where the theory is based on the principle of matching impeller-volute, which is then validated using three centrifugal pumps with specific speeds. Investigations into centrifugal pump experiments used as turbines (PAT) also have been conducted by [19][20]. The results of such experiments can be known and shown that the pump operates at a higher head and discharge value if it is synchronized in turbine mode and the best efficiency point (BEP) is lower than BEP in pump mode. Studies to increase the effectiveness of PAT applications, among others, have been carried out by [21][22].

Besides being able to be applied to micro hydro power plants, this PAT system is also widely used in energy recovery systems. The PAT is attached to the water distribution channel system to function as a water pressure reduction in the water line as well as a producer of electrical energy. Several PAT studies for applications on these water distribution line systems have been conducted by [23][24][25].

Most of the literature that discusses the prediction of pumps applied as turbines uses pumps with a centrifugal type. It is still rare to investigate mixed flow type pumps to be applied as PAT. This article discusses one way to find pump performance specifications when it is used as a turbine for micro hydro power plants using a pump with a mixed flow type. The numerical method by utilizing computational fluid dynamics (CFD) based software simulations that have been proven to be accurate according to previous studies was selected for use in obtaining predictions of pump characteristics as turbines. Then the PAT characteristics of the CFD simulation results are validated by conducting direct testing.

## II. Materials and Methods

Backflow pump testing to operate the pump as a turbine was carried out to test the results obtained from numerical simulations. Then, the data obtained by simulation and testing are compared to obtain validation of the analysis results. The mixed flow pump used as the object of this PAT research is the PN-Indra Surabaya type SB60-10 pump. This pump is an inventory of the Fluid Machinery Laboratory, FTMD ITB. The physical form of the pump is shown in Figure 1.

In modeling, the rear pump housing is called discharge and the front pump housing is called

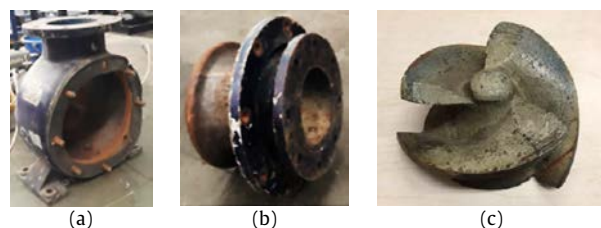


Figure 1. (a) Front pump housing; (b) Rear pump housing; (c) Impeller

Table 1.  
Mixed flow pump specification data

Material	Amount	Specification
Debit	150	m <sup>3</sup> /hour
Head	10	m
Power	7.46	kW
Rotational speed	2,000	rpm

Table 2.  
Mesh statistics

Statistic	Value
Node	2,451,941
Elements	4,683,249
Mesh metric	Orthogonal quality
Minimum	0.20235
Maximum	0.99998
Average	0.91322
Standard deviation	8.6438e-002

suction. In the pump catalog, there is pump specification data, including discharge, head, power, and rotational speed, as shown in Table 1. The next section is a simulation process using ANSYS Fluent software with a choice of Fluid Flow (Fluent) mode. The simulation process consists of four stages, namely Geometry, Mesh, Setup, and Solution & Result.

#### A. Geometry modeling

Fluid through the pump is modeled using the help of Solidworks software, then imported into ANSYS software for further simulation using Fluid Flow (Fluent). The pump model based on the modeling results is shown in Figure 2. Figure 2(a) is the isometric view of the pump model and Figure 2(b) is the piece/cutting side view. Figure 3 is the boundary condition for each computational model of the components. Figure 3(a) is the inlet fluid flow,

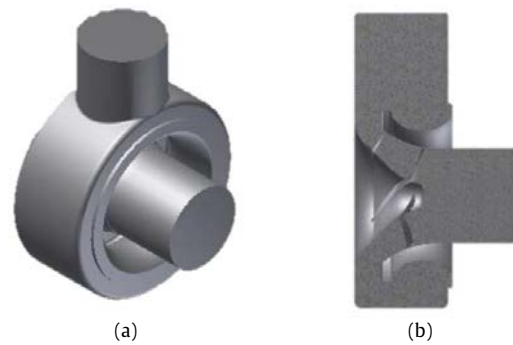


Figure 2. (a) Full view fluid volume; (b) Piece

Figure 3(b) is the outlet, and Figure 3(c) is the casing/wall. The blade boundary condition is shown in Figure 3(d), and the hub is shown in Figure 3(e).

#### B. Meshing process

At the meshing stage using tetrahedron mesh, the volume of fluid is divided into smaller elements. In the case of very complex geometries, these tetrahedral meshes are easy to generate and thus save a lot of time [26]. Because of that consideration, this type of mesh was chosen in this case. The meshing process is carried out using the default condition as the initial reference to produce mesh criteria that are considered in accordance with the physical condition of the model. It is simulated using a fluent solver with two criteria, namely skewness and minimum orthogonal quality. The average skewness score is 0.236 and the minimum qualifies mesh orthogonal quality is above 0.1, which is 0.17819. The meshing results of the computational pump model are shown in Figure 4.

The mesh statistics of the model are shown in Table 2. The mesh element in Table 2 is 4,683,249. Even though it is quite good in terms of skewness and orthogonality, this number of mesh elements needs a validation process in the next process with a mesh independence test so that the mesh elements are considered representative of the analysis process.

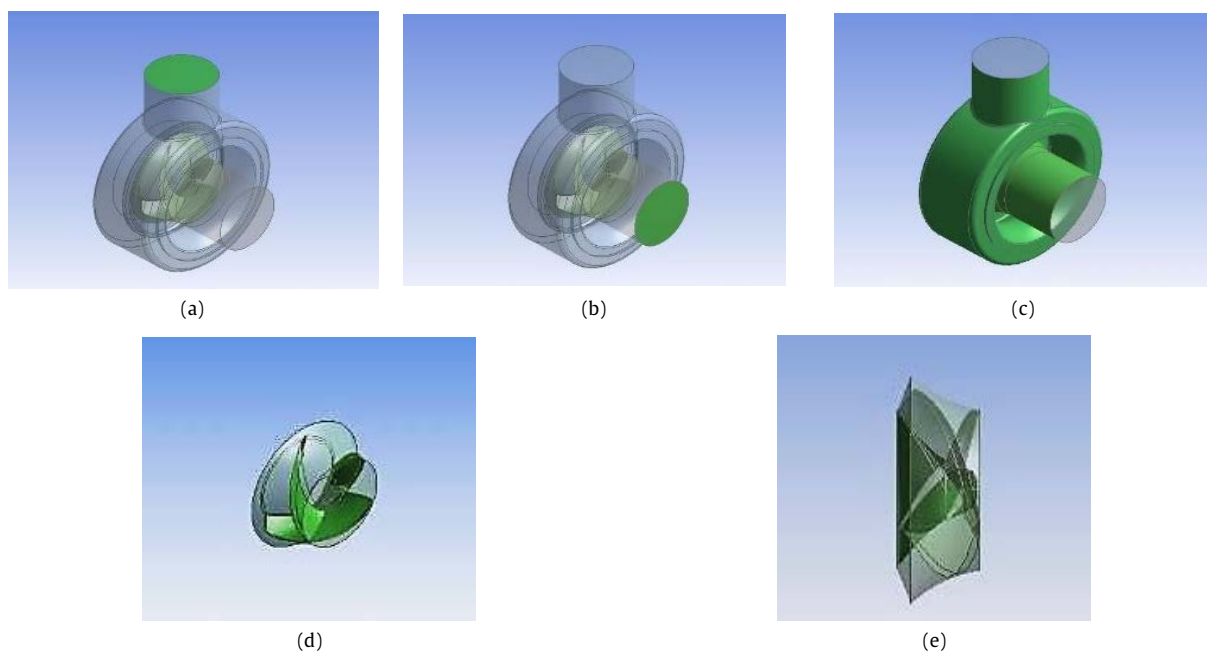


Figure 3. Named selection: (a) Inlet; (b) Outlet; (c) Casing; (d) Blade; (e) Hub

### C. Simulation settings

The setup stage is intended to make the initial setup before simulating using Fluent. In the processing options section, parallel (local machine) is selected and replaces the values contained in the solver processes column according to the capabilities of the computer used.

The arrangement is carried out in several categories contained in the solution stage consisting of selecting a scale into millimeters (mm), a steady condition, the gravity of -9.81 in columns Y, angular-velocity is changed to rpm, and the solver type is selected to pressure-based. On the Models menu, the viscous mode is selected. The models used are k-omega SST, Production limiter & constants model value for  $\alpha^*_{inf} = 1$ ,  $\alpha_{inf} = 0.52$ ,  $\beta^*_{inf} = 0.09$  and  $a1 = 0.31$ . The k-omega SST model is widely used in solving complex turbo engine problems and there are many walls where a boundary layer is formed due to the flow of fluid through it. The material used as the working fluid is water (water-liquid <h2O>) with a constant density of  $998.2 \text{ kg.m}^{-3}$  & a viscosity constant of  $0.001003 \text{ kg.m}^{-3}$ . In the Cell Zone Conditions menu, the parameters that are set are the material and movement behavior of each body. For discharge and suction, the material is arranged into water.

As for the impeller, in addition to adjusting the type of material to water, the rotational motion mode can be adjusted by selecting the frame motion option. The rotational motion of the impeller has a positive X rotary axis vector, so column X is assigned a value of 1 and the other axis is assigned a value of 0. The size of the impeller rotational speed is set in the rotational velocity section of the speed column (rpm) of 2,000 rpm. The relative specification chosen is absolute so that the reference of the rotary axis is a global coordinate defined in the geometry created.

Meanwhile, in the Boundary Conditions menu, the boundary conditions of the pump model are regulated as simulated as turbines. Setting boundary conditions including movement behavior on the walls of the blade and hub, as well as the pressure on the inlet and outlet sides of the pump. Blades and hubs are defined as walls that move with a rotating motion relative to the rotation of the impeller on the X-axis with a relative velocity magnitude of 0 rpm. It shows that the direction and rotational speed of the blade wall and hub are the same as the impeller, which is the reference of the two parts, so the moving wall motion is chosen, motion is chosen relative to adjacent cell zone-rotational, and the shear condition is chosen no slip with 0.5 wall roughness-constant.

The pressure on the outlet side is set by 0 Pa (gauge) by considering the outlet side as a reference to the size of the pump moved head. For pressure regulation on the inlet side, the pressure column is set as large as the head moved by the pump. In addition to the magnitude of the pressure value, the setting is also carried out by selecting the K and Omega modes, where K is the kinetic energy of turbulence,  $\omega$  = specific dissipation rate and I = intensity of turbulence. The values entered for

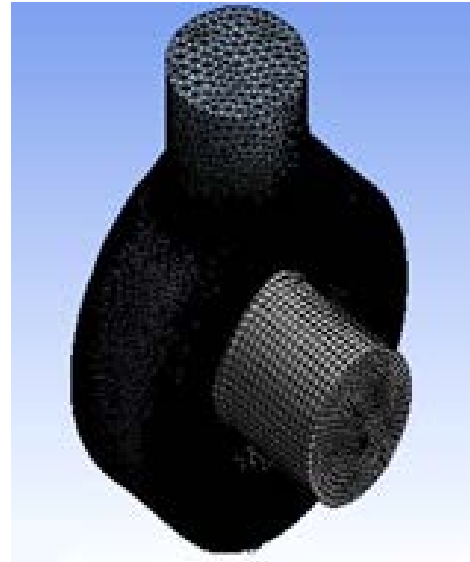


Figure 4. Meshing results

turbulent kinetic energy and specific dissipation rate use equation (1) and equation (2),

$$K = \frac{3}{2} (V_{avg} I)^2 \quad (1)$$

$$\omega = \frac{K^{0.5}}{C_{\mu}^{0.25} 0.09 D} \quad (2)$$

$C_{\mu}$  expresses a constant empirically whose value is 0.09. Using preliminary guesses of the average velocity on the inlet and outlet sides, the calculation results for turbulent kinetic energy were obtained by  $0.002155 \text{ m}^2.\text{s}^{-2}$ , and the specific dissipation rate was obtained by  $26.04661.\text{s}^{-2}$ . In the Turbo Topology menu, the definition is carried out on a surface named at the Geometry stage discussed earlier.

In solution initialization, the mode chosen is standard initialization, with compute from the selected side inlet and reference frame is absolute. Then, the Gauge pressure is filled with the inlet side pressure to be simulated of 97923.42 and Y-Velocity is filled with the initial guess of the flow speed on the inlet side by -4. After all the parameters in the input, then carry out the simulation running process by setting the number of iterations so that they converge.

### D. Installation experiment test

To assist in data collection in testing mixed flow pumps as turbines, several supporting equipment is needed, namely pumps, AC motors, gate valves, butterfly valves, flow meters, torsions, manometers, and tachometers. The test installation begins with drawing up a pump that will be used to drain the water in the pipeline and then flow into the PAT system. The series of test benches in the test installation can be seen through the PID diagram in Figure 5.

In Figure 6 of the pump installation arrangement, the pump shaft is connected to an AC motor or using a clutch. The suction pump is connected to the pipe until it is submerged in water, while the pump discharge part is connected to the gate valve, then the gate valve is connected to the reservoir using pipes and elbows.

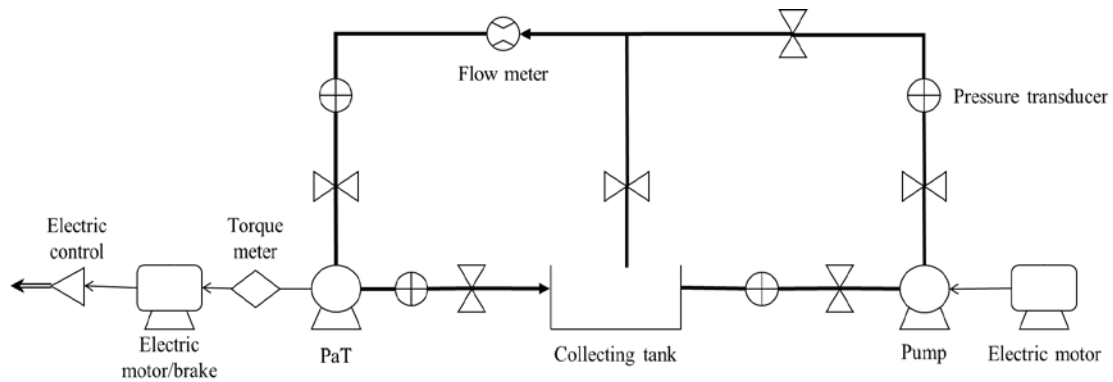


Figure 5. Test bench diagram

The arrangement of the PAT installation starts from the reservoir, pipe, and elbow to connect the butterfly valve. Then the butterfly valve is connected to the inlet side of the pump as turbine (PAT) using pipes and elbows. On the pipe is placed a flow meter to measure the flow rate of water in the pipe. In the inlet pipe and PAT outlet, a hole is attached to each tap and manometer. The torque meter is paired by means of being connected to the PAT shaft. The arrangement of the PAT installation is shown in Figure 7.

#### E. Testing work steps

The testing process begins with the position of the gate valve fully closed and the butterfly valve open. Then, the AC motor is turned on to run the pump. After 10 seconds, the gate valve is slowly opened until the water can begin to flow to fill the reservoir. Water will then flow past the butterfly valve to the inlet side of the PAT and enters the PAT, causing the PAT to work and the PAT shaft to rotate.

The manometer will show the pressure difference readings of the inlet side and the PAT outlet. The flow meter is turned on to a stable flow speed. The torque meter begins to have functioned until the rotating speed of the PAT shaft is reduced to 800 rpm and 400 rpm. The data taken are the rotating speed of the PAT shaft, the torque generated, the pressure difference of the inlet and outlet sides, and the speed of water flow in the pipeline.

### III. Results and Discussions

#### A. Simulation results

The iteration process of convergent immolation is achieved after the residual values of continuity, x-y-z velocity, k, and omega have passed the specified error limit. The iteration data are in the form of torque as shown in Table 3. From these data it can be seen that the total torque is -38.80641 Nm with a total coefficient of -0.99503614.

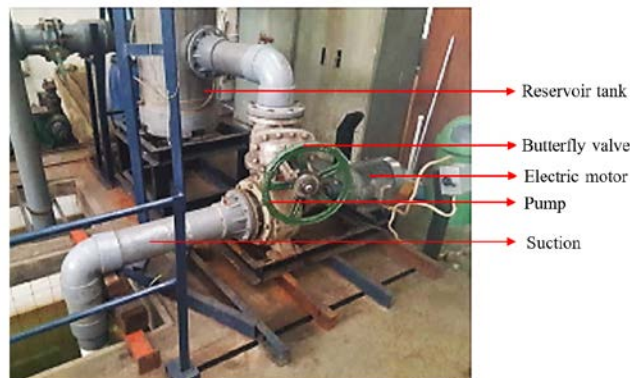


Figure 6. Assembly of pump



Figure 7. Assembly of PAT

Table 3.  
Torque output results of moments-moment center (0 0 0) moment axis (1 0 0)

Zone	Moments (n-m)			Coefficients		
	Pressure	Viscous	Total	Pressure	Viscous	Total
Wall-28	0	0	0	0	0	0
Wall-27	0	0.00013802982	0.00013802983	0	3.5392265e-06	3.5392265e-06
Wall-25	3.8660795e-07	-5.5352484e-06	-5.5352484e-06	9.9130242e-09	-1.4192944e-07	-1.3201642e-07
Wall-24	2.4576884e-06	5.9013209e-06	8.3590094e-06	6.3017651e-08	1.5131952e-07	2.1433357e-07
Blade	-43.9333	0.32219332	-43.611107	-1.1264948	0.0082613671	-1.1182335
Hub	-0.0035930499	0.12629554	0.12988859	9.2129484e-05	0.003238347	0.003330476
Casing-discharge-solid	-0.049116374	0.0018930088	-0.047223364	-0.0012593942	4.8538687e-05	-0.0012108555
Casing-suction	-3.8783185e-07	5.0647869	5.0647869	-9.9444067e-09	0.12986633	0.12986632
Casing-discharge-solid	-0.20231247	-0.16026746	-0.16026746	-0.0051874991	0.001078077	-0.0041094221
Casing-impeller	-0.0033532127	-0.17927596	-0.18262917	-8.5979812e-05	-0.0045968194	-0.0046827992
Net	-44.184487	5.3780762	-38.80641	-1.1329355	0.13789939	-0.99503614

The iteration data in the form of the mass rate is shown in Table 4. From the data in the table, it can be seen that there is no significant difference between the mass flow at the inlet and outlet, where the inlet is 74.07208 Kg/s and the outlet is 74.27893 Kg/s.

The data that has been obtained is collected for each rotational speed. The simulations were performed at 400, 800, 1480, 1800, and 2000 rpm. However, the data shown in table form are only the turbine discharge, head, power, and efficiency at 400 and 800 rpm in Table 5 and Table 6. The data in the two tables are then loaded into a graph shown in Figures 8-10.

#### B. Validation of numerical simulation results

To prove that the simulation that has been carried out is valid, a mesh independency test process is carried out. In this process, the number of mesh elements is varied against a variable that will be taken as data, namely the mass rate of flow. The purpose of the mesh independency test is to see the number of elements that are considered representative for later use in the analysis process. The results of the mesh independency test are shown in Table 7.

It can be seen from the results of the mesh independency test that the more the number of mesh elements, the mass rate obtained will be smaller. At the change in the number of mesh elements of 4,683,249 to 5,428,728, it can be seen

that the change in the mass rate is very small; the decrease is only 0.638 %. Therefore, the number of mesh elements of 4,683,249 can be used for the numerical simulations.

#### C. Simulation result analysis

Any numerical simulation data that has been obtained can be processed into various points that can be arranged into regression curves that can describe the characteristics of PAT. The curves of the PAT numerical simulation results for various rotating speeds and performance parameters are shown in Figures 8-10.

Figure 8 shows the curve graph of power vs. discharge. It can be seen that PAT has demonstrated characteristics that correspond to the theoretical basis. The curve for each rotating speed tends to be linear, then for each rotating speed that increases, the gradient of the curve also increases. However, this does not directly mean that efficiency will also increase, and it should be looked at further on the efficiency vs. discharge curve.

Figure 9 shows that PAT demonstrated characteristics corresponding to the theoretical basis. The curve for each rotating speed tends to be linear, then for each rotating speed that increases, the gradient of the curve also increases. This suggests that at an increased rotating speed of PAT and for the same flow discharge, the torque generated will be greater. However, this does not directly mean that efficiency will also increase, and it should be looked at further on the efficiency vs. discharge curve.

Table 4.  
Mass rate output result

Parameters	Value		Unit
	Inlet	Outlet	
Mass flow	74.07208	74.27893	kg/s
Swirl Number	-1.34498	-0.68598	-
Average total pressure	120000	1203.964	Pa
Average radial flow angle	-89.9994	6.846271	deg
Average theta flow angle	-51.0569	30.13422	deg
Engr. passage loss coefficient	-12.34489	-	-
Norm. passage loss coefficient	0.989967	-	-
Efficiency-hydraulic	20.74779	-	%
Axial forces	-1810.518	-	Nm
Torque	-43.66385	-	N
Average	Mass-weighted		-

Table 5.  
Numerical simulation data PAT 400 rpm

Q (m <sup>3</sup> /h)	H (m)	P (W)	$\eta$ (%)
266.66	12.13	1,617.37	18.38
255.04	11.12	1,434.62	18.60
238.22	9.90	1,242.79	19.37
221.66	8.59	1,087.94	21.01
197.86	7.08	873.88	22.95
180.05	6.07	767.14	25.82
160.79	5.06	635.04	28.71
138.10	4.05	473.43	31.13
112.14	3.04	319.49	34.46
83.99	2.03	160.39	34.61
45.05	1.02	5.68	4.56

Table 6. Numerical simulation data PAT 800 rpm

Q (m <sup>3</sup> /h)	H (m)	P (W)	η (%)
242.23	13.15	2,588.27	29.88
232.34	12.14	2,349.16	30.62
215.96	11.14	2,124.46	32.48
201.12	9.92	1,870.00	34.48
189.30	9.12	1,645.06	35.05
176.44	8.11	1,449.23	37.26
160.26	7.10	1,108.96	35.86
140.71	6.09	738.90	31.73
117.65	5.08	547.19	33.69
95.26	4.07	284.79	27.04
58.01	3.06	26.73	5.54

Table 7. Results of the mesh independency test

Σ Mesh element	Mass rate (kg/m)	Error (%)
3,572,720	54.9988	-
3,878,440	51.846	5.731
4,683,249	49.921	3.712
5,428,728	49.6031	0.638

Figure 10 shows a parabolic curve with a critical point in the form of a maximum point. For an increased PAT rotating speed, the curve will shift towards the right. Meanwhile, the maximum efficiency value of each rotating speed does not differ much, which ranges from 35 % to 40 %. The discharge indicating the maximum efficiency point on the curve is the PAT operating point for each

rotating speed. From the discharge, the PAT head and power indicating the PAT operating point for each rotating speed can also be determined when returning to the head vs. discharge curve and the power vs. discharge curve.

The PAT operating points are indicated by a square-shaped symbol on each curve and are also shown in Table 8. Based on the data shown in Table 8, the optimal operating point of each turbine rotation is directly proportional to the value of each test parameter.

If a comparison of the pump performance curve and PAT is carried out, the simulation results are in one graph, where the pump curve is displayed on the positive absciss and the PAT curve on the negative absciss. This curve is shown in Figure 11.

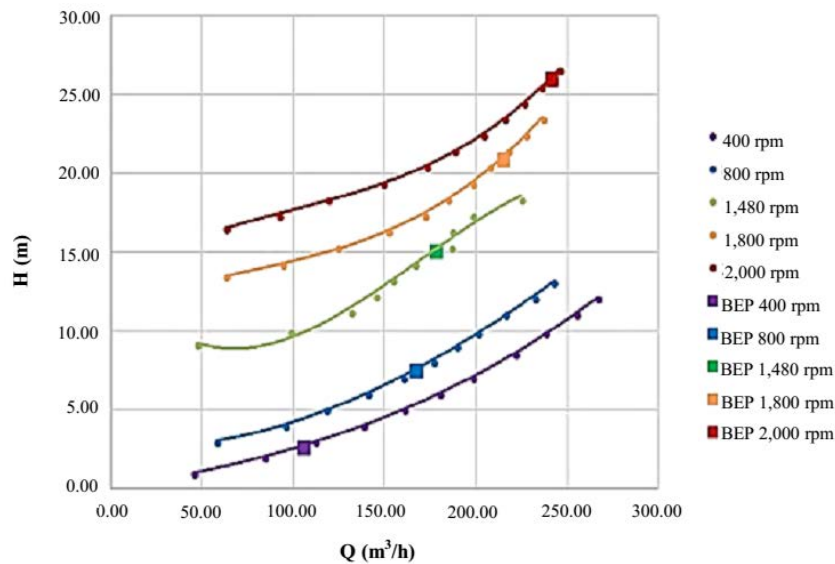


Figure 8. Head vs. PAT discharge for various rotating speeds

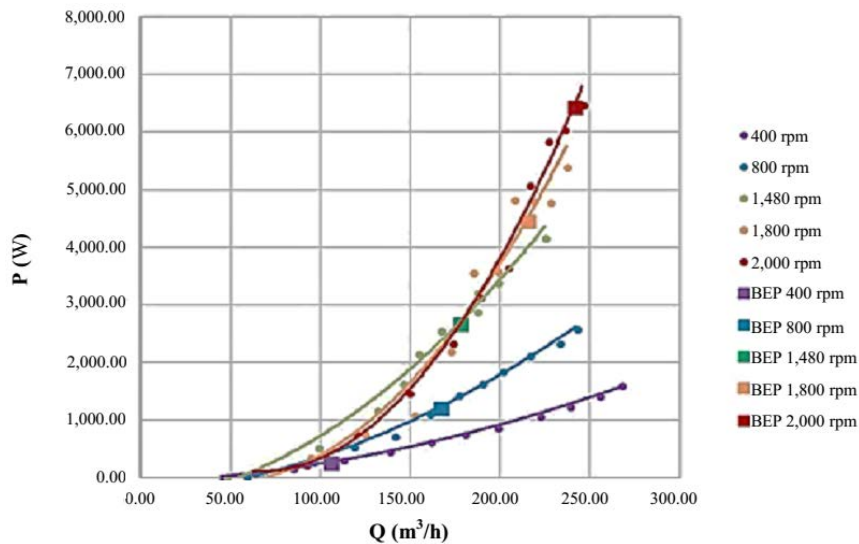


Figure 9. Power vs. debit of PAT discharge for various rotating speeds

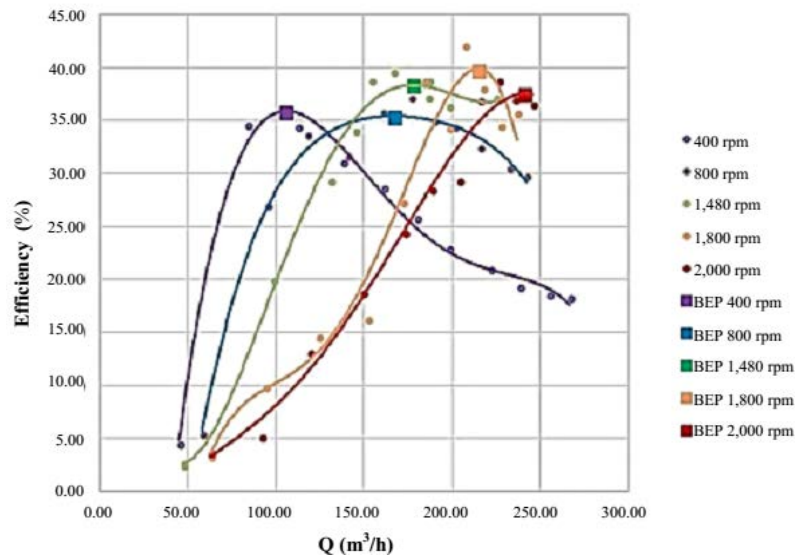


Figure 10. Efficiency vs. debit of PAT discharge for various rotating speeds

Based on the curve obtained in Figure 11, it shows that the trend of the curve tends to decrease in each BEP. This is due to a decrease in the head ( $H$ ), which is directly proportional to the increase in discharge ( $Q$ ).

Based on the comparison of the head vs. discharge curve of the pump and the PAT obtained, the value of the pump operating point and PAT at various rotating speeds can be known through Table 9. Based on the curves and table above, it can be seen that for the same rotating speed, the PAT has an operating point at a lower discharge compared to the operating point of the pump, but at a larger head. Then, for the same one rotating speed, the highest efficiency of the PAT is also lower than the highest efficiency of the pump.

#### D. Blade pressure contour analysis

Figure 12 (a) shows the pressure contours on the rear at side view, while Figure 12 (b) shows the isometric view of the impeller. The simulation results show that the maximum pressure contours are  $1,227 \times 10^5$  Pa and the minimum pressure contours are  $-1,401,105$  Pa. In these two pictures show the contours of the pressure on the PAT

impeller blade. In both images, in contrast to dynamic pumps in general, it can be seen that the flow of water entering through the PAT mashes the blade and hub parts of the impeller thoroughly. This can be understood because the inlet channel is in the radial direction and its located perpendicular to the rotary axis of the impeller, in contrast to dynamic pumps which generally have blade-offending channels. This results in a stream of water pounding the hub will cause losses because the impact located perpendicular to the rotating axis of the impeller causes the moment arm on the impeller not to form, so that the energy from the flow cannot be converted into the desired torque. This factor can also be used as a reason for the low efficiency of PAT in this mixed flow pump.

#### E. PAT test results

Tests performed on mixed flow pumps as turbines can only be performed for rotational speeds of 400 rpm and 800 rpm. This is due to the limitations of the testing equipment, where the pump used for testing is only able to provide a maximum head of 2 meters for load less PAT rotation. The PAT test data are shown in Table 10

Table 8.  
PAT optimal operating points at various rotating speeds.

rpm	Optimal operating point			
	Q (m <sup>3</sup> /h)	H (m)	Power (W)	Efficiency (%)
400	104.80	2.79	281.33	35.98
800	166.23	7.63	1.231.56	35.52
1,480	177.12	15.22	2.704.28	38.48
1,800	214.21	21.04	4.483.75	39.87
2,000	240.52	26.13	6.456.83	37.63

Table 9.  
Comparison of pump and PAT operating points at various rotating speeds

rpm	Pump			PAT		
	Q (m <sup>3</sup> /h)	H (m)	Efficiency (%)	Q (m <sup>3</sup> /h)	H (m)	Efficiency (%)
1,480	228.28	4.46	54.58	-177.12	15.22	38.48
1,800	268.24	6.81	59.17	-214.21	21.04	39.87
2,000	310.14	8.13	61.13	-240.52	26.13	37.63

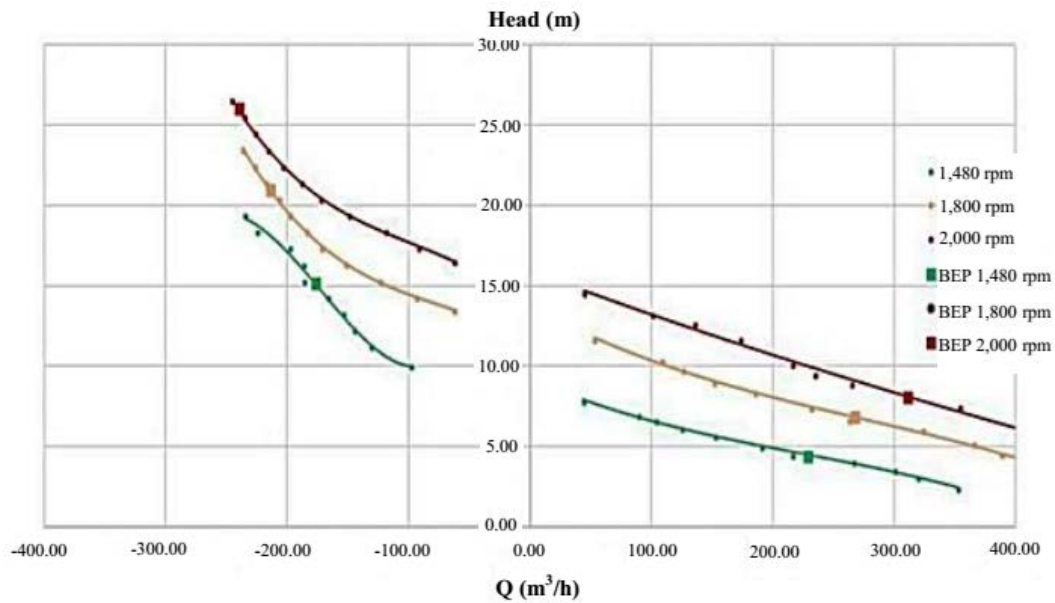


Figure 11. Curve head vs debit of discharge pump and PAT

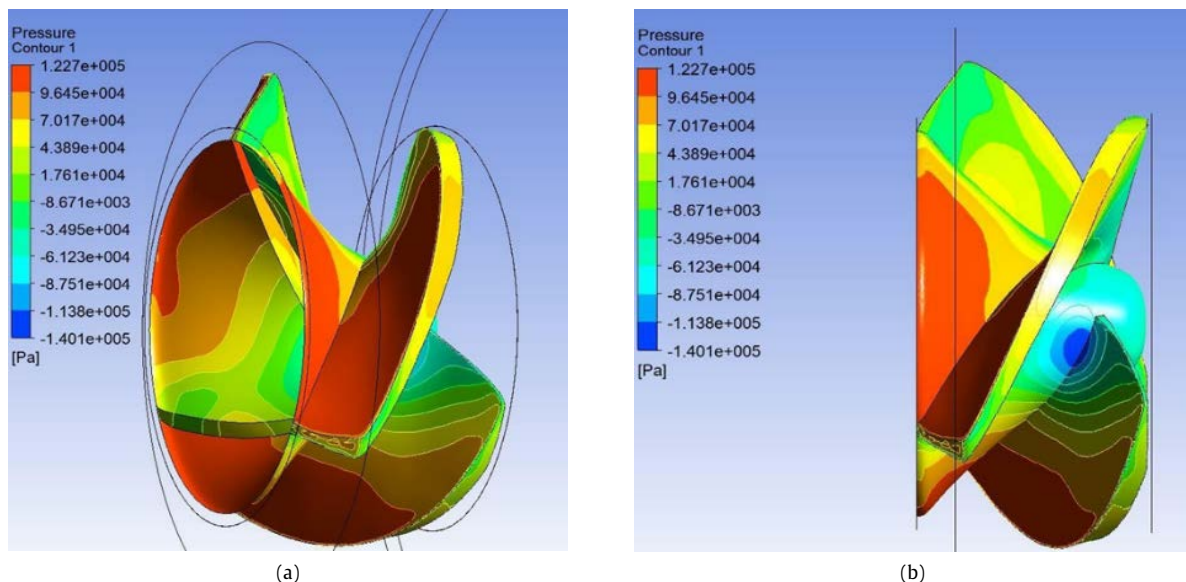


Figure 12. Pressure contours on the rear: (a) side view; (b) isometric view impeller

and Table 11. Table 10 shows the simulation results in the form of discharge, head, power and turbine efficiency at 400 rpm. Table 11 shows the simulation results in the form of discharge, head, power and turbine efficiency at 800 rpm where the data in the two tables are then loaded into a graph shown in Figure 13, Figure 14, and Figure 15.

#### F. Analysis of test results

The results of tests carried out on the PAT show that for the head, power, and discharge at a rotational speed of 400 rpm, it is not so much different from the curve of the simulation results, but for other parameters, each rpm is quite far different. The most noticeable differences are the head and discharge for a rotational speed of 800 rpm, as well as the efficiency of each rotating speed. The test results in various factors that result in losses in PAT operations. The most important disadvantage is friction on the shaft. This is because, in numerical simulations, the PAT shaft and its supporting components, such as bearings and

Table 10.  
Test data on PAT at a rotational speed of 400 rpm

Q (m <sup>3</sup> /h)	H (m)	P (W)	$\eta$ (%)
51.88	0.82	10.89	9.42
74.21	1.51	21.33	7.00
73.55	1.83	23.16	6.30
70.92	1.95	22.99	6.10
74.21	1.91	26.28	6.80
51.88	0.78	10.85	9.85
73.55	1.47	21.04	7.15
72.89	1.77	22.88	6.52
70.27	1.90	22.71	6.25
73.55	1.87	25.93	6.91
51.22	0.77	10.66	9.98
72.89	1.45	20.81	7.21
72.24	1.78	22.63	6.45
69.61	1.90	22.46	6.24
72.89	1.89	25.71	6.86

Table 11.  
Test data on PAT at a rotational speed of 800 rpm

Q (m <sup>3</sup> /h)	H (m)	P (W)	η (%)
76.18	1.23	13.06	5.11
76.83	1.51	18.24	5.78
76.18	1.61	20.45	6.11
76.83	1.68	20.60	5.87
75.52	1.15	12.78	5.38
76.18	1.45	18.14	6.01
75.52	1.58	20.12	6.17
76.18	1.62	20.28	6.02
74.86	1.18	12.81	5.32
75.52	1.43	17.82	6.06
74.86	1.58	20.00	6.19
75.52	1.61	20.16	6.08

lubricants, are not modeled. A comparison of the performance of the test results with the simulation results can be seen in Figure 13, Figure 14, and

Figure 15. Based on the test and simulation analysis graphs, as seen in Figure 13, the comparison between the head (H) and discharge (Q) trend graph tends to increase during testing and simulation. While in Figure 14, the test analysis graph between power (P) and discharge (Q) shows that the trend tends to increase both at the time of testing and simulation.

The graph of test analysis and simulation of efficiency (η) to discharge (Q) is shown in Figure 15. The simulation results show that the efficiency of each PAT rotating speed tends to increase from discharge 49 m<sup>3</sup>/h to 110 m<sup>3</sup>/h. PAT efficiency with a speed of 400 rpm began to decrease after passing discharge above 110 m<sup>3</sup>/h. Meanwhile, the PAT efficiency with a speed of 800 rpm only started to decline after the water debit was above 175 m<sup>3</sup>/h. The experimental results show that efficiency tends to increase as the flow rate increases. This shows conformity with the simulation results. However, it has not been validated as to what discharge the efficiency of each PAT cycle will decrease.

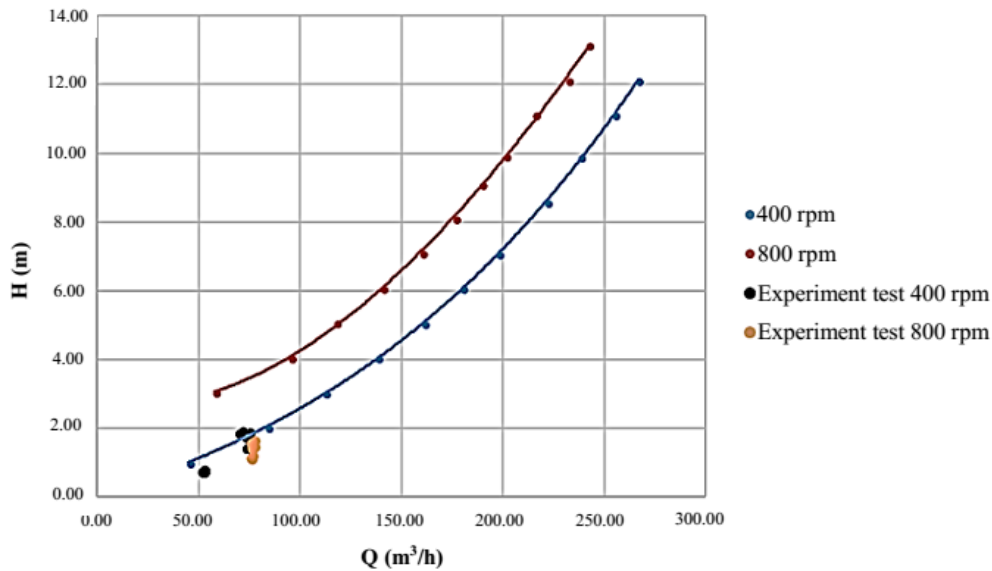


Figure 13. Comparison curve of head vs discharge test and simulation results

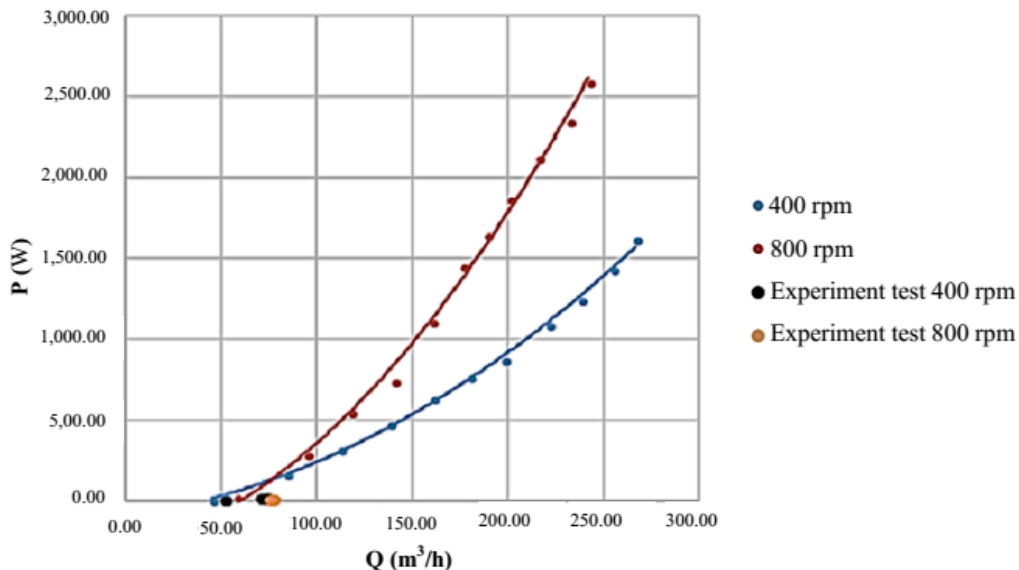


Figure 14. Power vs discharge comparison curve of test and simulation results

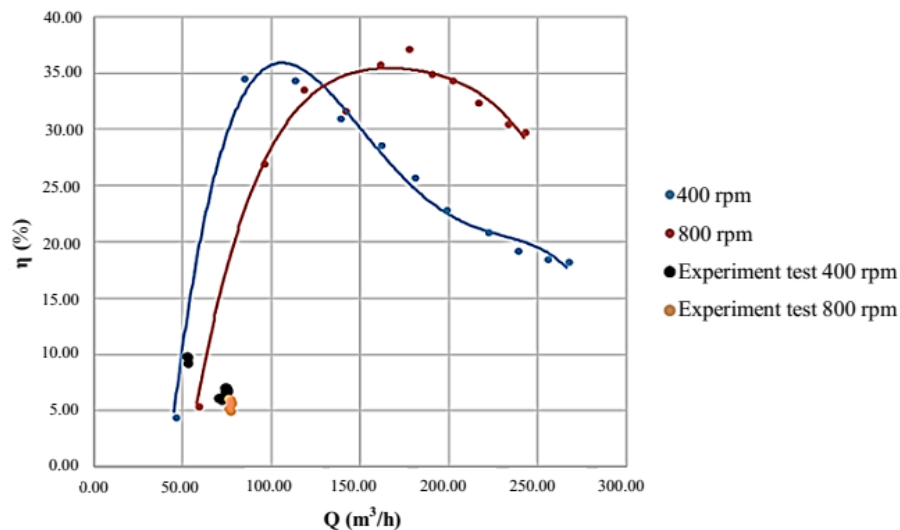


Figure 15. Head vs discharge comparison curve of test and simulation results

## IV. Conclusion

This paper has discussed a method for predicting the performance characteristics of a mixed flow type pump when applied as a turbine (PAT) for remote rural micro hydro applications. Research to predict the performance of a mixed flow pump which is operated as a turbine at various rotational speeds is carried out using the CFD numerical simulation method. The results obtained are shown in a performance curve. It is known that the highest efficiency for each rotating speed ranges from 35–40 %. The validation of the numerical simulation results is carried out by conducting experiments. The test results show the characteristics of PAT, namely the performance range that is close to the results of the numerical simulation with a difference of 10 %. To get more convincing simulation validation results, it is recommended to carry out more simulations in the range of rotational speed/flow rate variations according to the rotational speed of the test equipment capacity. Experimental work by connecting a PAT with a generator is considered for further work.

## Acknowledgments

Our gratitude goes to Mr. Ir. I Nengah Diasta, M.T., for the permission given to use the the material for this research and to publish this paper. We would like to thank also to all those who have helped and supported in the process of preparing this manuscript.

## Declarations

### Author contribution

S. Mejiartono: Writing - Original Draft, Writing - Review & Editing, Conceptualization, Formal analysis, Investigation, Visualization, Resources, Software. M.F. Hikmawan: Writing - Original Draft, Writing - Review & Editing, Conceptualization, Formal analysis, Investigation, Visualization, Resources, Software. A.S. Nugraha: Visualization, Supervision.

## Funding statement

This research did not receive any specific grant from funding agencies in the public, commercial, or not-for-profit sectors.

## Competing interest

The authors declare that they have no known competing financial interests or personal relationships that could have appeared to influence the work reported in this paper.

## Additional information

Reprints and permission: information is available at <https://mev.lipi.go.id/>.

Publisher's Note: National Research and Innovation Agency (BRIN) remains neutral with regard to jurisdictional claims in published maps and institutional affiliations.

## References

- [1] E. Erdiwansyah, M. Mahidin, H. Husin, N. Nasaruddin, K. Khairil, M. Zaki, et al., "Investigation of availability, demand, targets, and development of renewable energy in 2017–2050: a case study in Indonesia," *International Journal of Coal Science & Technology*, vol. 8, pp. 483–499, 2021.
- [2] Y. E. Unutmaz, A. Demirci, S. M. Tercan, and R. Yumurtaci, "Electrical energy demand forecasting using artificial neural network," in *2021 3rd International Congress on Human-Computer Interaction, Optimization and Robotic Applications (HORA)*, pp. 1–6, 2021.
- [3] I. W. Ngarayana, J. Sutanto, and K. Murakami, "Predicting the future of Indonesia: energy, economic and sustainable environment development," in *IOP Conference Series: Earth and Environmental Science*, p. 012038, 2021.
- [4] A. S. Ahmar, "A comparison of  $\alpha$ -Sutte indicator and Arima methods in renewable energy forecasting in Indonesia," *Int. J. Eng. Technol*, vol. 7, pp. 20–22, 2018.
- [5] R. A. Subekti, "Survey potensi pembangkit listrik tenaga mikro hidro di Kuta Malaka kabupaten Aceh Besar Propinsi Nanggroe Aceh Darussalam," *Journal of Mechatronics, Electrical Power, and Vehicular Technology*, vol. 1, pp. 5–12, 2012.
- [6] E. K. Bawan, A. D. Palintin, and E. A. Patandianan, "Analisis potensi energi terbarukan pembangkit listrik tenaga mikrohidro di Manokwari Selatan," *Jurnal Penelitian Sainstek*, vol. 26, pp. 24–34, 2021.
- [7] M. A. Isa, P. Sudjono, T. Sato, N. Onda, I. Endo, A. Takada, et al., "Assessing the sustainable development of micro-hydro power plants in an isolated traditional village West Java, Indonesia," *Energies*, vol. 14, p. 6456, 2021.
- [8] A. Morabito and P. Hendrick, "Pump as turbine applied to micro energy storage and smart water grids: A case study,"

- Applied energy*, vol. 241, pp. 567-579, 2019.
- [9] M. Stefanizzi, T. Capurso, G. Balacco, M. Binetti, S. M. Camporeale, and M. Torresi, "Selection, control and techno-economic feasibility of pumps as turbines in water distribution networks," *Renewable Energy*, vol. 162, pp. 1292-1306, 2020.
- [10] F. Plua, V. Hidalgo, P. A. López-Jiménez, and M. Pérez-Sánchez, "Analysis of applicability of CFD numerical studies applied to problem when pump working as turbine," *Water*, vol. 13, p. 2134, 2021.
- [11] D. Stefan, M. Rossi, M. Hudec, P. Rudolf, A. Nigro, and M. Renzi, "Study of the internal flow field in a pump-as-turbine (PaT): Numerical investigation, overall performance prediction model and velocity vector analysis," *Renewable Energy*, vol. 156, pp. 158-172, 2020.
- [12] X. Su, S. Huang, X. Zhang, and S. Yang, "Numerical research on unsteady flow rate characteristics of pump as turbine," *Renewable Energy*, vol. 94, pp. 488-495, 2016.
- [13] S. Abazariyan, R. Rafee, and S. Derakhshan, "Experimental study of viscosity effects on a pump as turbine performance," *Renewable Energy*, vol. 127, pp. 539-547, 2018.
- [14] S. Yang, F. Kong, W. Jiang, and X. Qu, "Research on rotational speed to the influence of pump as turbine," in *IOP Conference Series: Earth and Environmental Science*, p. 042023, 2012.
- [15] M. M. Ghorani, M. H. S. Haghighi, A. Maleki, and A. Riasi, "A numerical study on mechanisms of energy dissipation in a pump as turbine (PAT) using entropy generation theory," *Renewable Energy*, vol. 162, pp. 1036-1053, 2020.
- [16] S. S. Yang, S. Derakhshan, and F. Y. Kong, "Theoretical, numerical and experimental prediction of pump as turbine performance," *Renewable Energy*, vol. 48, pp. 507-513, 2012.
- [17] D. Zariatin, D. Rahmalina, E. Prasetyo, A. Suwandi, and M. Sumardi, "The effect of surface roughness of the impeller to the performance of pump as turbine pico power plant," *Journal of Mechanical Engineering and Sciences*, vol. 13, pp. 4693-4703, 2019.
- [18] T. Lin, Z. Zhu, X. Li, J. Li, and Y. Lin, "Theoretical, experimental, and numerical methods to predict the best efficiency point of centrifugal pump as turbine," *Renewable Energy*, vol. 168, pp. 31-44, 2021.
- [19] Y. Han and L. Tan, "Influence of rotating speed on tip leakage vortex in a mixed flow pump as turbine at pump mode," *Renewable Energy*, vol. 162, pp. 144-150, 2020.
- [20] J. C. Alberizzi, M. Renzi, M. Righetti, G. R. Pisaturo, and M. Rossi, "Speed and pressure controls of pumps-as-turbines installed in branch of water-distribution network subjected to highly variable flow rates," *Energies*, vol. 12, p. 4738, 2019.
- [21] O. Fecarotta, H. M. Ramos, S. Derakhshan, G. Del Giudice, and A. Carravetta, "Fine tuning a PAT hydropower plant in a water supply network to improve system effectiveness," *Journal of Water Resources Planning and Management*, vol. 144, p. 04018038, 2018.
- [22] M. Perez-Sanchez, F. J. Sánchez-Romero, H. M. Ramos, and P. A. López-Jiménez, "Improved planning of energy recovery in water systems using a new analytic approach to PAT performance curves," *Water*, vol. 12, p. 468, 2020.
- [23] M. Postacchini, G. Darvini, F. Finizio, L. Pelagalli, L. Soldini, and E. Di Giuseppe, "Hydropower generation through pump as turbine: Experimental study and potential application to small-scale WDN," *Water*, vol. 12, p. 958, 2020.
- [24] A. Carravetta, L. Antipodi, U. Golia, and O. Fecarotta, "Energy saving in a water supply network by coupling a pump and a pump as turbine (PAT) in a turbopump," *Water*, vol. 9, p. 62, 2017.
- [25] M. Rossi, M. Righetti, and M. Renzi, "Pump-as-Turbine for energy recovery applications: the case study of an aqueduct," *Energy Procedia*, vol. 101, pp. 1207-1214, 2016.
- [26] M. Sosnowski, J. Krzywanski, K. Grabowska, and R. Gnatowska, "Polyhedral meshing in numerical analysis of conjugate heat transfer," in *EPJ Web of Conferences*, p. 02096, 2018.